Hindawi
Advances in Materials Science and Engineering
Volume 2022, Article ID 2474374, 12 pages
https://doi.org/10.1155/2022/2474374

Research Article

Property Characterization of Anti-Aging Additives and Modified Asphalt Based on Long-Term Aging Behavior

Junlong Liu,[1,2] Lijing Chu,[3] Tianyuan Zhao,[4] Yunchu Zhu,[5] Zhi Cang,[6] Qian Chen,[1,2] and Junshen Yuan[5]

[1]*School of Highway, Chang'an University, Xi'an 710064, China*
[2]*Key Laboratory of Road Structure & Material of Transport Ministry, Chang'an University, Xi'an 710064, China*
[3]*Guangzhou Urban Planning & Design Survey Research Institute, Guangzhou 510060, China*
[4]*Guangdong Nanyue Transportation Investment & Construction Co. Ltd, Guangzhou 510000, China*
[5]*School of Civil and Transportation Engineering, Guangdong University of Technology, Guangzhou 510006, China*
[6]*Datongbei Expressway Management Co. Ltd, Shanxi Transportation Holding Group Co. Ltd, Taiyuan 030006, China*

Correspondence should be addressed to Qian Chen; 2016121160@chd.edu.cn

Received 20 July 2022; Accepted 18 August 2022; Published 8 September 2022

Academic Editor: Wenke Huang

In order to achieve the good application of hindered amine light stabilizer (HALS) in the long-term aging control of asphalt pavement material, Tinuvin770 and Tinuvin622 light stabilizers were selected as modifiers for asphalt. The microstructure and characteristics of hindered amine light stabilizers were characterized by FIB-SEM. The elemental composition and relative content of hindered amine light stabilizers were studied by means of EDS analysis. The functional group composition of hindered amine light stabilizers was analyzed based on Dynamic-FTIR. On this basis, light stabilizer modified asphalt was prepared, and the effect of hindered amine light stabilizer on the thermal rheological properties of asphalt binder during UV aging period was studied by dynamic shear rheology (DSR). The changing law of low temperature rheological properties of hindered amine light stabilizer modified asphalt was evaluated by low temperature bending beam rheological test (BBR). The results showed that the hindered amine light stabilizer could capture the free radicals formed during the photodegradation of asphalt when subjected to ultraviolet aging. Under the impact of ultraviolet aging, hindered amine light stabilizer could improve the high temperature performance of asphalt binder. Furthermore, HALS could achieve the improving effect on the low temperature rheological properties and long-term aging performance of asphalt pavement materials.

1. Introduction

One of the reasons for the long-term aging of asphalt pavement is that the ultraviolet energy radiation intensity is high, which leads to the significant photo-oxidation reaction of asphalt [1, 2]. Ultraviolet rays can be divided into long wave, medium wave, and short wave according to the wavelength range. The ultraviolet energy in the wavelength is similar to the bond energy of the main molecular bonds C-H, C-C, and C=C of asphalt [3, 4]. When ultraviolet rays irradiate the asphalt surface, the photon energy in the ultraviolet rays will destroy the internal molecular bonds of the asphalt, induce free radical reactions, and cause the transformation of internal light components to heavy components, resulting in the instability of the asphalt colloid structure and finally causing cracks and pits in the asphalt pavement. There are grooves and other diseases [5]. Therefore, in view of the problem of ultraviolet aging of asphalt pavement, it is urgent to find an effective means to control the aging process of asphalt to delay the occurrence of pavement failures, which is of great significance for improving the service life of asphalt pavement [6–9]. The existing methods for improving the anti-aging performance of asphalt are mainly realized by adding modifiers [10–12]. Commonly used anti-ultraviolet aging modifiers mainly include carbon black, nanomaterials, intercalation materials and ultraviolet light absorbers, and so on, which improve the anti-

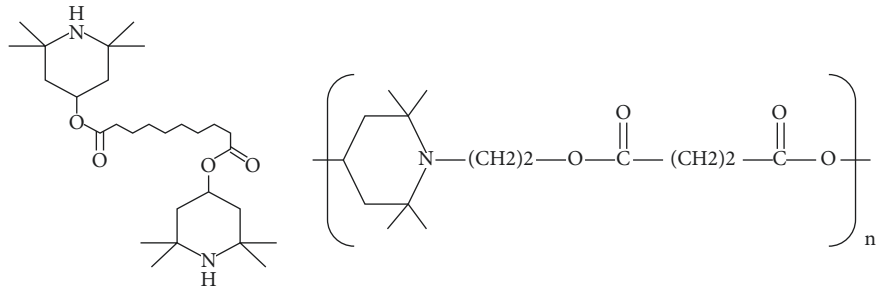

Figure 1: Molecular structure of T770 and T662 light stabilizers.

Table 1: Technical properties of light stabilizer.

Light stabilizer	Melting point (°C)	Molecular weight	Density (g/cm^3)
T770	84	480.72	1.01
T622	365	129.2	1.05

Table 2: Technical properties of 70# base asphalt.

Indices	Testing results	Specification
Penetration/0.1 mm	63.1	T0604-2011
Ductility (10°C) cm	19.3	T0605-2011
Softening point (°C)	46.9	T0606-2011

Table 3: Setting UV aging time.

Outdoor UV aging time	3 months (h)	6 months (h)	9 months (h)	12 months (h)
Indoor UV aging time	76.25	152.5	228	305

aging performance of asphalt by shielding or absorbing ultraviolet rays [13–15]. However, there are still some problems in the modification application of existing additives to asphalt, for example, the low temperature performance improvement effect of asphalt is not good. In contrast, light stabilizers could effectively control asphalt aging, have good compatibility with asphalt, and have good application prospects in asphalt UV aging control [16–18].

Based on this, Tinuvin770 and Tinuvin622 light stabilizers were selected as modifiers in this study. The microscopic morphology and characteristics of hindered amine light stabilizers were characterized by FIB-SEM. The elemental composition and relative content of hindered amine light stabilizers were studied by means of EDS spectroscopy. The functional group composition and characteristics of hindered amine light stabilizers were comprehensively analyzed based on Dynamic-FTIR. Light stabilizer modified asphalt was prepared, and the effect of hindered amine light stabilizer on high temperature rheological properties of asphalt binder during UV aging was systematically studied by dynamic shear rheology (DSR). The change law of low temperature rheological properties of hindered amine light stabilizer modified asphalt under ultraviolet aging conditions was evaluated by low temperature bending beam rheological test, which provided a scientific basis for the application and popularization of hindered amine light stabilizer in pavement engineering.

2. Materials and Methods

2.1. Materials

2.1.1. Hindered Amine Light Stabilizers. Tinuvin770 and Tinuvin622 hindered amine light stabilizers are preferred as asphalt modifiers, and the molecular structures of T770 and T662 light stabilizers are shown in Figure 1. The mechanism of action of hindered amine light stabilizers was to capture the free radicals formed during the photodegradation of asphalt during ultraviolet aging through the hindered amine structure of the modifier, thereby playing the role of anti-ultraviolet aging. The dosage of T770 and T662 was 2%, 4%, and 6% by the asphalt mass. The technical indices are shown in Table 1.

2.1.2. Asphalt. 70# asphalt was selected as the carrier for Tinuvin770 and Tinuvin622 light stabilizers, and the technical indices are shown in Table 2.

2.2. Preparation Process of Light Stabilizer Modified Asphalt. 70# asphalt was heated to 130°C and kept for 1 h. Then, according to the planned dosage, the light stabilizer modifier was weighted and added into the molten asphalt. After mixing, the mixture of asphalt and light stabilizer was stirred at 130°C for 1 h. The stirring speed of mixture was about 1000 rad/min. After stirring, the light stabilizer modified asphalt was finished preparing.

2.3. Methodology

2.3.1. UV Aging Method. The UV radiation was simulated indoor by using UV light lamp, whose power was approximately 300 W. Concerning that the UV radiation area of lamp was about 0.8 m^2, the ultraviolet radiation intensity could be calculated and the specific calculated value was about 375 W/m^2. The conversion formula of outdoor and indoor UV radiation was shown in formula (1). The transformed UV aging time is shown in Table 3.

Figure 2: Focused ion beam scanning electron microscope and gold sprayer.

Figure 3: Thermogravimetric-infrared spectroscopy system.

$$\text{Indoor simulation time} = \frac{\text{outdoor solar radiation energy}}{\text{power of indoor UV radiation}} \quad (1)$$

2.3.2. FIB-SEM Test. The microstructure of hindered amine light stabilizers was analyzed by focused ion beam field emission scanning electron microscope (Figure 2). The elemental composition and content of hindered amine light stabilizers were analyzed by EDS spectroscopy. The sample of hindered amine light stabilizer powder was placed on an aluminum plate, and the sample was sprayed with gold. Then, scanning electron microscope was used to magnify 2000, 4000, and 10000 times, respectively, to observe the microscopic morphology of the sample surface.

2.3.3. FTIR Analysis. The functional group composition of T770 and T622 light stabilizers was analyzed by TG thermogravimetric-infrared spectroscopy system (Figure 3). The number of test scans was 32, and the resolution was 40 cm^{-1}. Tests were carried out under nitrogen atmosphere.

2.3.4. LAS Test. The LAS test was performed using Anton Paar SMART PAV dynamic shear rheometer (Figure 4). The test temperature was 18°C, and the distance between the 8 mm plates was 1 mm. Frequency sweep adopts the control strain mode, the strain was 0.1%, the sweep frequency range was 0.2 ~ 30 Hz, and the shear modulus and phase angle of each frequency were recorded. The amplitude sweep adopted

Figure 4: Dynamic shear rheometer.

the controlled strain mode, the loading frequency was 10 Hz, and the sample was preloaded for 100 cycles for the period of 10 seconds at the strain ;of 0.1%. The continuous loading with the linear increase of 1% in strain levels of 1 to 30% was performed for 100 cycles (10 s) for each strain level, and the total time was 310 s.

2.3.5. BBR Test. The low temperature bending beam rheometer was used to test the creep stiffness S and creep rate *m* of light stabilizer modified asphalt under different

Figure 5: Low temperature bending beam rheometer.

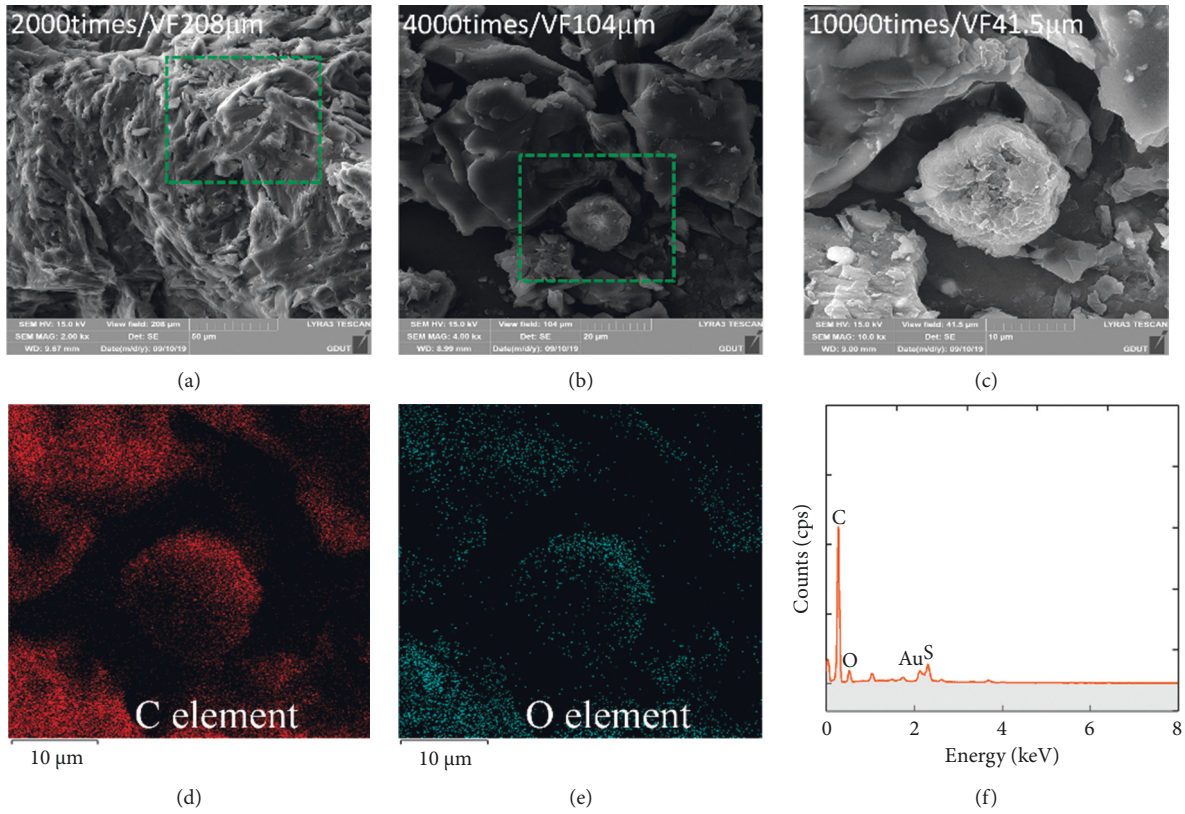

Figure 6: Micromorphology and elemental composition of T770 light stabilizer. (a) 2000 times. (b) 4000 times. (c) 10000 times. (d, e) Element mapping diagrams. (f) EDS energy spectrum.

UV aging times. Cannon's TE-BBR bending beam rheometer (Figure 5) was used for the test, referring to the specific test method of ASTM D6648-01. The test temperature is −12°C, and the creep stiffness S and creep rate m of the light stabilizer modified asphalt at 60 s were tested.

3. Results and Discussion

3.1. Analysis of Micromorphology and Elemental Composition of Light Stabilizers. It could be seen from the observation of the micro-morphological characterization results of T770 light stabilizer (Figure 6) that when the magnification was 2000 times, the surface of T770 light stabilizer was dense. At the same time, there were slight depressions and holes on the surface of T770 light stabilizer, and the roughness was relatively high, combined with asphalt. The asphalt could be fully integrated, forming an effective structure and improving the stability of the modified asphalt. In the 4000 times result, it could be seen that the surface of T770 was mainly composed of large-sized and smooth block-like structures, and the pores were embedded with granular substances of different sizes. When the granular material was further magnified to 10,000 times, it was found that the

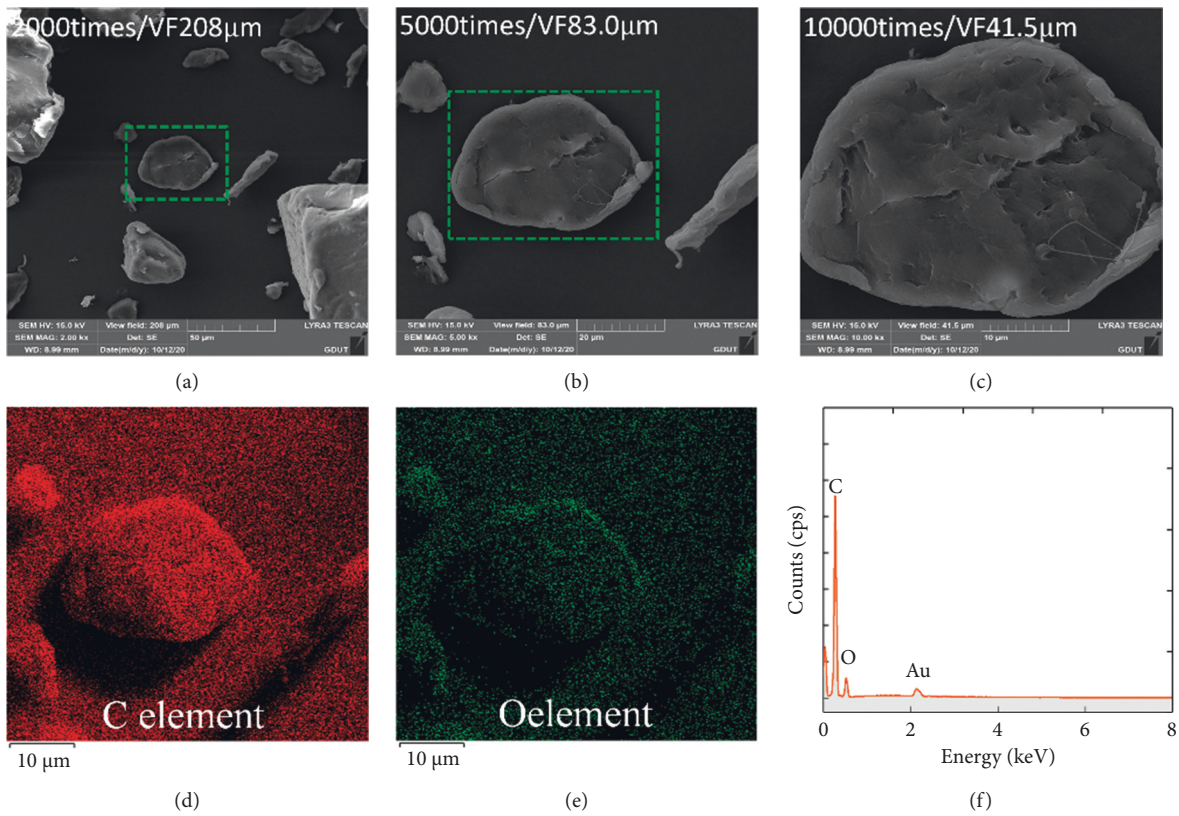

Figure 7: The microscopic morphology and elemental composition of T622 light stabilizer. (a) 2000 times. (b) 5000 times. (c) 10000 times. (d, e) Element mapping diagram. (f) EDS energy spectrum.

surface of the material was formed by superimposing micron-sized particles and aggregated to the middle area. Figures 6(d)–6(f) show that T770 light stabilizer was mainly composed of C and O, and there were trace elements such as S.

Under the magnification of 2000 times (Figure 7), the T622 light stabilizer had irregular structures such as rod-like structures, but mainly circular structures. After magnifying to 5000 times (Figure 7(b)), it could be observed that there were horizontal and vertical cracks in the middle position, which indicated that the surface of the T622 structure had certain undulations and roughness changes. Under the observation of 10000 times (Figure 7(c)), there were many cracks, grooves, pits, and laminated structures on the surface of T622 light stabilizer. Figures 7(d)–7(f) verify that the constituent elements of T622 were mainly C and O, and its element content corresponded to the structural formula, which was close to the element distribution of T770.

3.2. Dynamic-FTIR Analysis. It could be seen from the analysis in Figure 8 that in the first 20 minutes of the test, no substance escaped during the heating process of T770 light stabilizer, and the intensity was relatively stable. When the time exceeded 20 min, the GS curve rose to certain extent, which indicated that the connection strength between the unstable structure of T770 light stabilizer and the host gradually deteriorated with the passage of time and temperature. The rising curve at 36.09 min might be due to the change of GS intensity caused by the escape of impurities such as carbon dioxide. Correspondingly, in the infrared spectrum, it could be seen that there is a weak peak at the wavenumber of 1500 cm^{-1}. Starting from 42.73 min, the GS intensity curve of T770 light stabilizer rose rapidly. In the infrared spectrum corresponding to 2929.37 cm^{-1}, a strong characteristic peak formed by the anti-symmetric stretching vibration of methylene appears, as well as olefin C-H vibrational absorption peak at 1454.39 cm^{-1} and 1375.66 cm^{-1} wavenumbers. As the temperature continued to rise, the reaction rate of T770 light stabilizer reached the peak at this time and then decreased rapidly. When the heating time exceeded 50.05 min, the GS curves tended to be flat, and the intensity of the characteristic peaks also weakened, but the specific wavenumber positions of the characteristic peaks did not change.

From the analysis in Figure 9, it could be seen that the T622 light stabilizer was always in a flat stage within 28 minutes after the start of the test, which indicated that no or very little substances were detected during this period, and the intensity is basically at the zero-scale level. As the time continued to change, the GS intensity curve changed accordingly. Take the infrared spectra of three characteristic time points, namely, 29.28 min (intensity begins to change), 33.36 min (intensity reaches the maximum

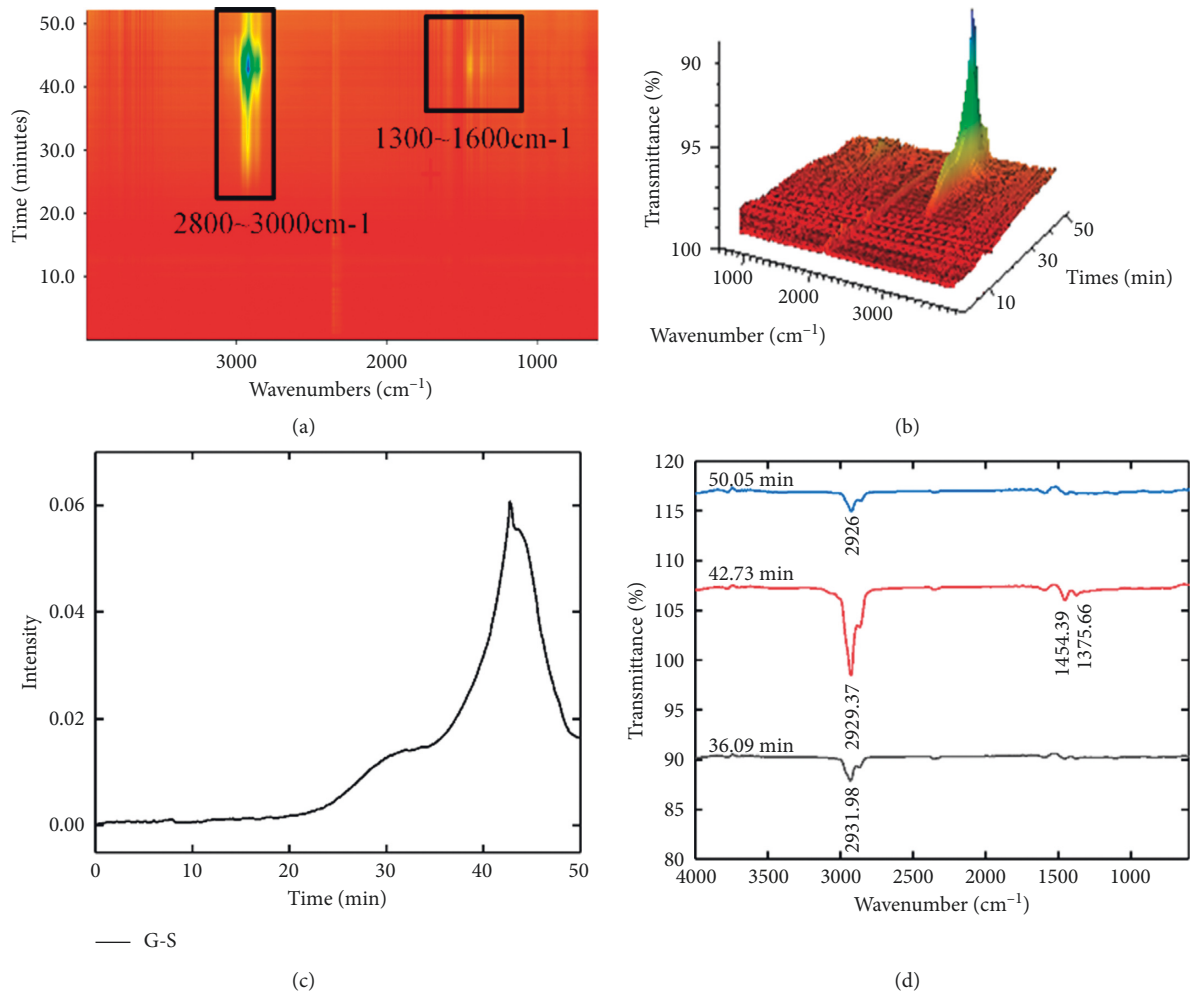

Figure 8: Dynamic-FTIR analysis results of T770. (a) 2D. (b) 3D. (c) GS. (d) Absorption.

value), and 39.32 min (intensity drops to minimum value). When the test time reached 29.28 min, the GS intensity curve changed. Accompanied by the production and escape of different substances, there were also several characteristic peaks with low intensity in the spectrum, among which 1809.86 cm^{-1} and 1044.18 cm^{-1} were the C=O bond stretching vibrations of acid anhydride and the C-O of saturated fatty acid anhydride, respectively. When the test time reached 33.36 min, the GS curve reached the maximum intensity. The intensity of the characteristic peak in the spectrum increased significantly, among which 2974.58 cm^{-1} represented the methyl characteristic peak, and 1751.17 cm^{-1} and two characteristic peaks in the range of 1050 ~ 1300 cm^{-1} represented the C=O bond pull of the ester group. It exhibits extensive vibration absorption peaks. When the time exceeded 39.32 min, the intensity curve had been flattened. At the same time, the absorption peak in the spectral curve became smaller, and the corresponding positions of the characteristic peaks were almost unchanged.

3.3. LAS Test Analysis. It could be seen from the analysis in Figure 10 that stress peaks appeared in the LAS curve of the matrix asphalt under different UV aging times, but the change range of the stress-strain curve was weak, and the growth rate before reaching the peak was lower than that of the other four kinds of modified asphalt. After the peak was reached, it decreased rapidly and became flat. In contrast, the matrix asphalt with UV aging for 152.5 h had the stress peak phenomenon, but there was a secondary peak change at the peak, and then the peak decreased. In the LAS curve of the 228 h UV-aging asphalt, the appearance of the peak was compared with that of the 152.5 h asphalt specimen, when the stress value reduced to the lowest value was also reduced to about 5%.

It could be analyzed from the stress-strain curve in Figure 11 that the yield stress of T770 modified asphalt with UV aging for 76.25 h reached the maximum value and was quite different from the yield stress of the asphalt specimens at the other three aging time points. The yield stress gradually decreased with the extension of UV

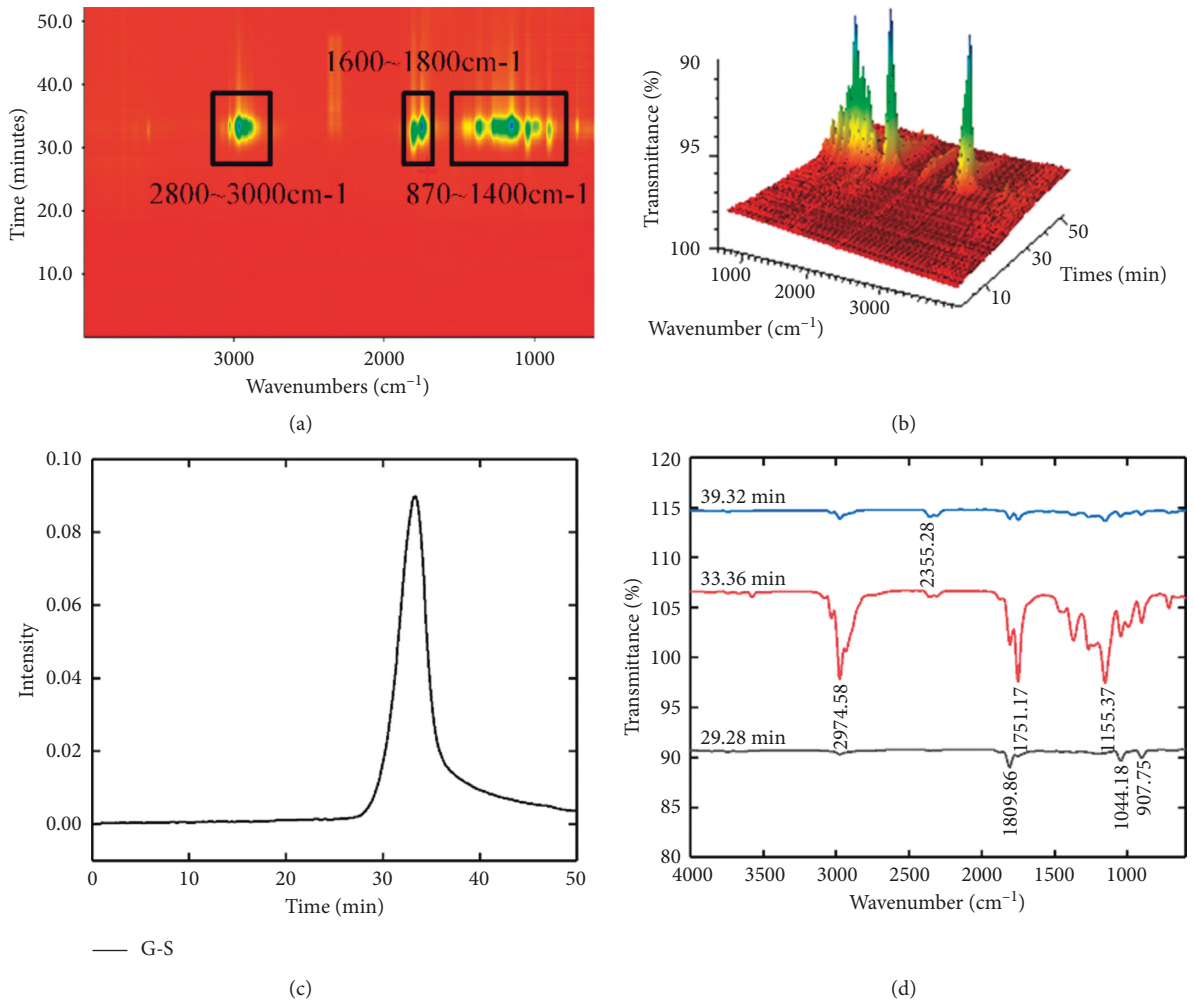

Figure 9: Dynamic-FTIR analysis results of T662. (a) 2D. (b) 3D. (c) GS. (d) Absorption.

radiation time. When the UV radiation time was higher than 152.5 h, the yield stress value of T770 modified asphalt dropped sharply at 2.5% strain and dropped to the horizontal line at 5% strain. From 76.25 h to 152.5 h, the damage degree of T770 modified asphalt increased rapidly. With the UV aging time extending to 305 h, the damage degree of T770 modified asphalt decreased slowly. In addition, except for 76.25 h, the curves of asphalt at the other three aging time points in the curve were all within the strain range of 3% to 8%, the stress appeared to be stable for a short time, and the time for stress maintenance did not reflect the relevant laws.

It could be analyzed from Figure 12 that the peak value of shear stress of T622 modified asphalt with UV aging for 76.25 h was the smallest among the four aging time points, which was about 56.4 kPa, and the corresponding strain value was about 1.27%. Then, the shear stress reached the maximum value at 152.5 h, which was about 199 kPa, and its strain value was 1.95%. The stress peak value of the latter was nearly four times that of the former, and the strain value was only 0.68% higher than that of the former. The fatigue performance of T622 asphalt corresponding to UV aging for 152.5 h was the lowest, and the fatigue performance of asphalt corresponding to the UV aging time was recovered to some extent. In addition, through the comparison of Figures 12(b)–12(d), it could be analyzed that the size of the strain value gradually decreased to the vicinity of the zero value and tended to be flat with the prolongation of the ultraviolet aging time.

3.4. BBR Test Analysis. It could be seen from the analysis in Figure 13 and Table 4 that under different UV aging times, the creep modulus of T622 and T770 modified asphalt was less than that of 70# asphalt, and the creep rate was greater than that of 70# asphalt, which indicated that T622 and T770 modifiers could improve the low temperature performance of asphalt directly. Following the extension of UV aging time, the creep modulus of different asphalts all showed an upward trend, while the creep rate gradually decreased, which demonstrated that in the UV aging range of 76.25 h to 305 h, the prolongation of UV aging time would reduce the low temperature performance of asphalt. While the UV aging time was extended from 76.25 h to 152.5 h, 228 h, and 305 h, for

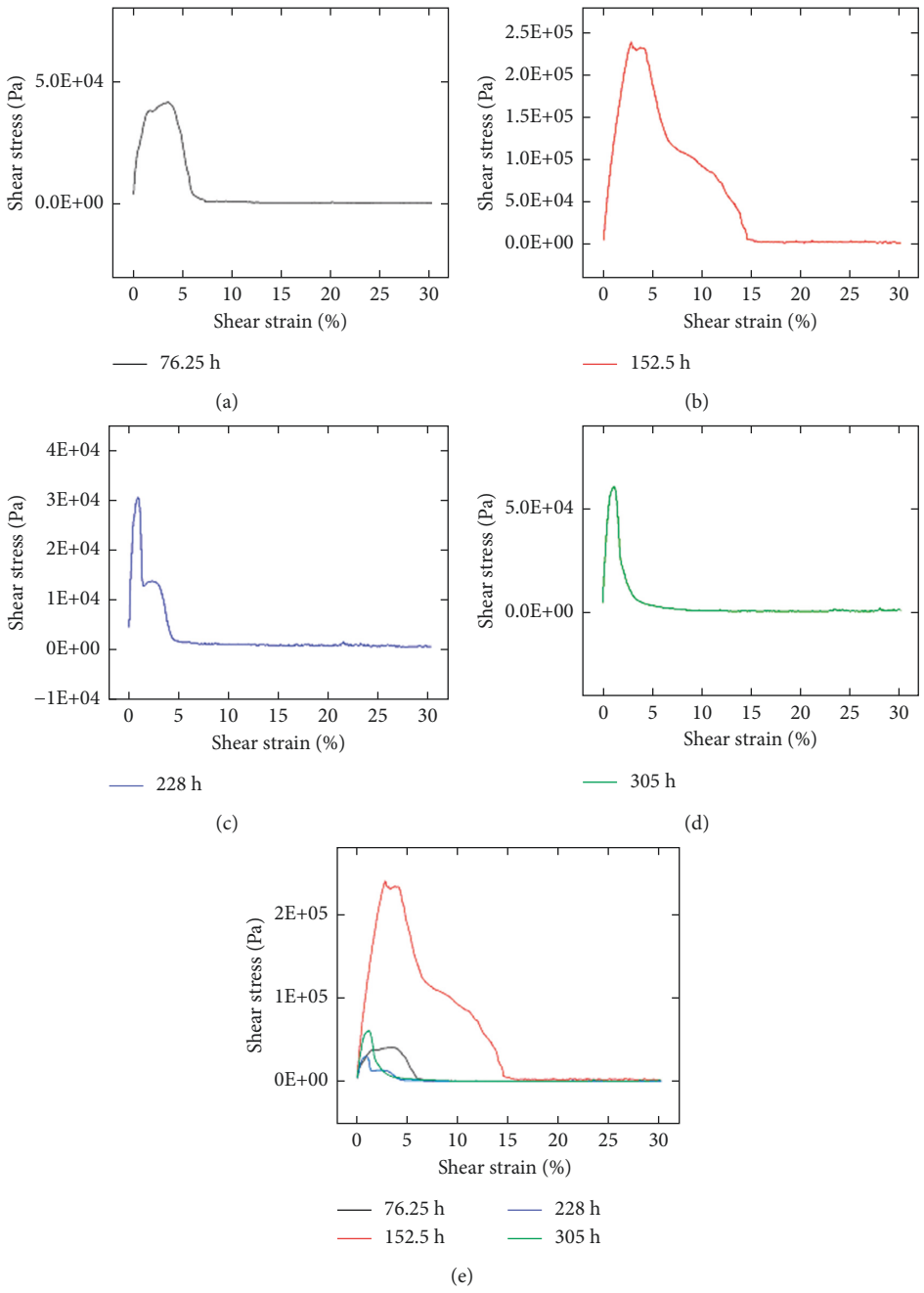

Figure 10: LAS results of 70# asphalt subjected to different UV aging times.

70# asphalt, the creep modulus S increased by 12%, 21%, and 25%, and the creep rate m decreased by 6%, 11%, and 15%, respectively. For T622 modified asphalt, the creep modulus S increased by 7%, 12%, and 20%, and the creep rate m decreased by 2%, 5%, and 8%, respectively. The increasing rate of creep modulus S and the decreasing rate of creep rate m were significantly smaller than those of 70# asphalt.

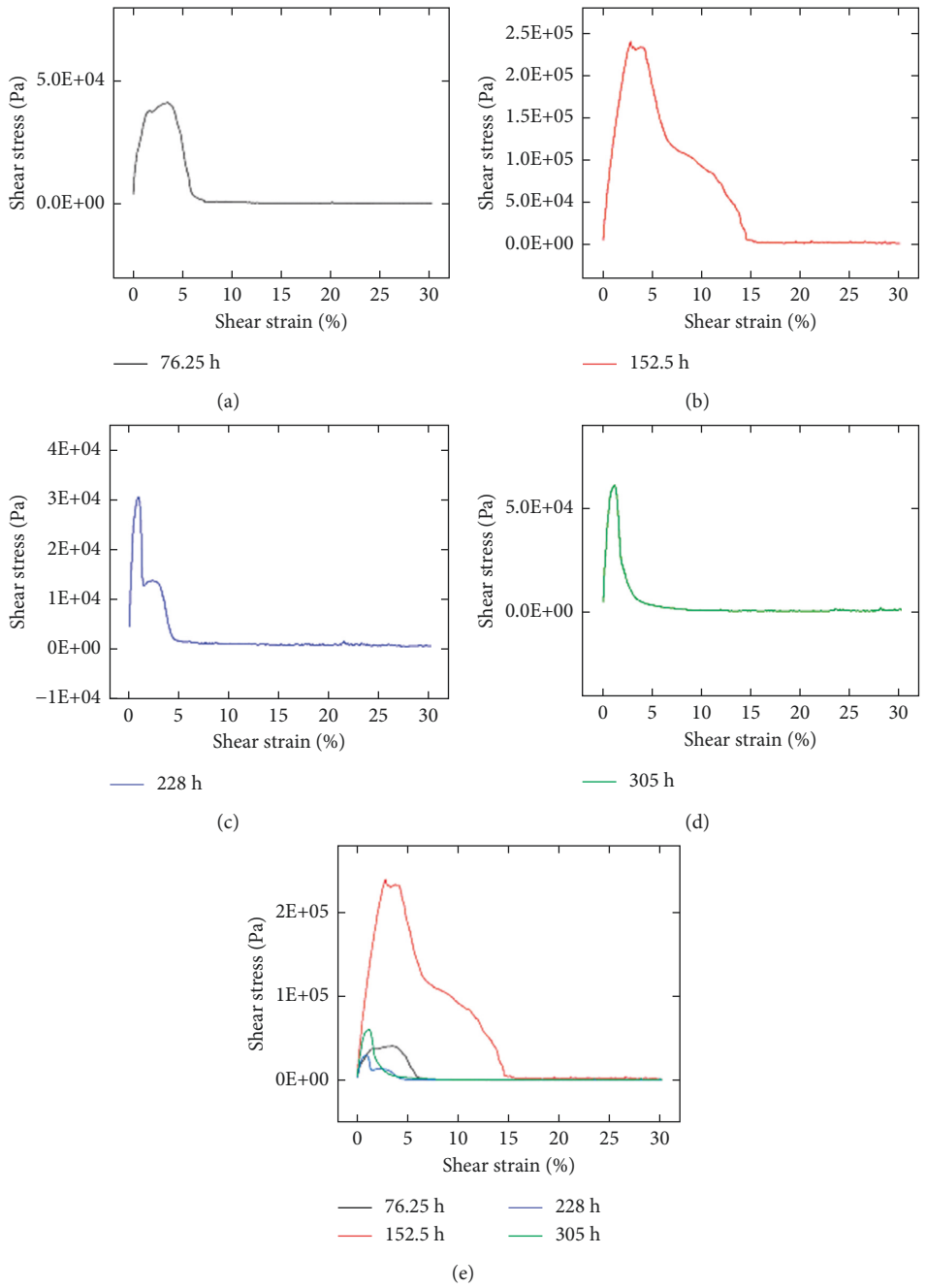

Figure 11: LAS results of T770 modified asphalt subjected to different UV aging times.

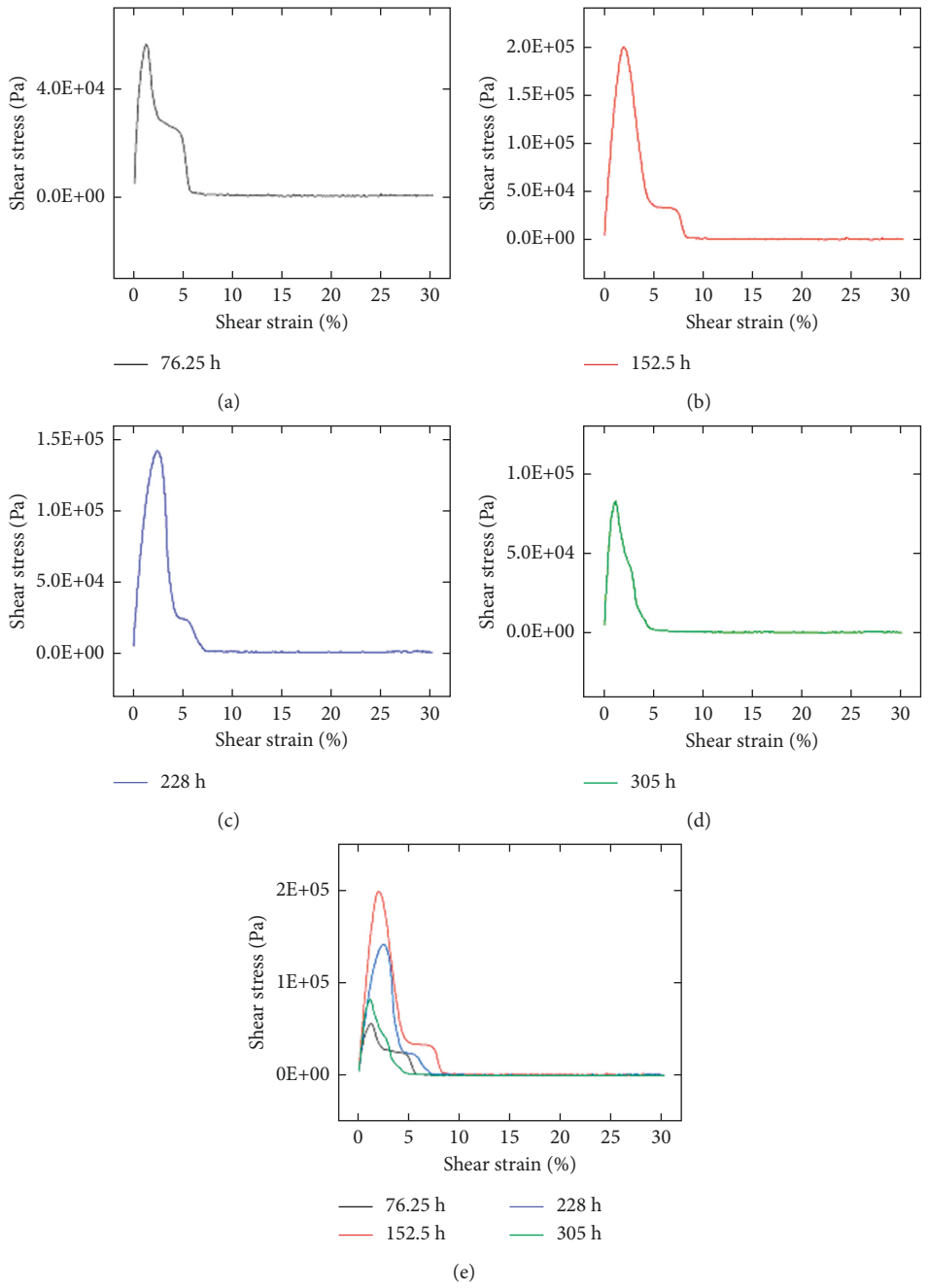

Figure 12: LAS results of T622 modified asphalt subjected to different UV aging times.

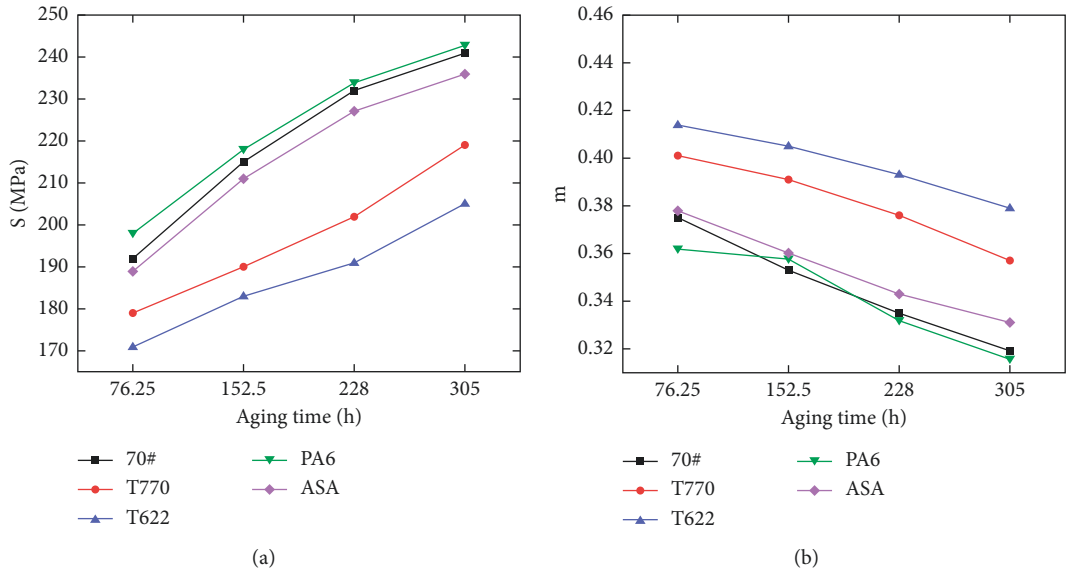

(a) (b)

Figure 13: BBR bending beam rheological test results. (a) The relationship between the creep modulus S and aging time of different kinds of asphalt. (b) The relationship between the creep rate m and aging time of different kinds of asphalt.

Table 4: BBR bending beam rheological test results.

Asphalt type	76.25 h		152.5 h		228h		305 h	
	S/MPa	*m*	S/MPa	*m*	S/MPa	*m*	S/MPa	*m*
70#	192	0.372	215	0.353	232	0.335	241	0.319
T770	179	0.401	190	0.391	202	0.376	219	0.357
T662	171	0.414	183	0.405	191	0.393	205	0.379

4. Conclusions

(i) The surface of T770 light stabilizer was dense and there were slight depressions and holes at the same time. The roughness of surface was relatively high. T622 light stabilizer had irregular structures such as rod-like structures, but mainly circular structures. The constituent elements of T622 were mainly C and O, and its element content corresponded to the structural formula, which was close to the element distribution of T770.

(ii) In the infrared spectrum corresponding to 2929.37 cm^{-1}, a strong characteristic peak formed by the anti-symmetric stretching vibration of methylene appears, as well as olefin C-H vibrational absorption peak at 1454.39 and 1375.66 cm^{-1} wavenumbers. With the continuous change of time, the GS intensity curve of T622 light stabilizer changed correspondingly.

(iii) The yield stress gradually decreased with the extension of UV radiation time. The shear stress peak of T622 modified asphalt aged for 76.25 h was the smallest among the four aging time points, which was about 56.4 kPa, and the corresponding strain value was about 1.27%. Then, the shear stress reached the maximum value at 152.5 h, about 199 kPa, and its strain value was 1.95%.

(iv) Under different UV aging times, the creep modulus of T622 and T770 modified asphalt was less than that of 70# asphalt, and the creep rate was greater than that of 70# asphalt, which indicated that T622 and T770 modifiers could directly improve the low temperature performance of asphalt.

Data Availability

The data used to support the findings of this study are available from the corresponding author upon request.

Conflicts of Interest

The authors declare that they have no conflicts of interest.

Acknowledgments

This study was sponsored by the Fundamental Research Funds for the Central Universities, CHD (300102212516), and Special Fund for Science and Technology Innovation Strategy of Guangdong Province (nos. pdjh2021a0149 and pdjh2022b0161). The authors are grateful for the support.

References

[1] H. L. Zhang and D. Zhang, "Effect of Different inorganic nanoparticles on physical and ultraviolet aging properties of bitumen," *Journal of Materials in Civil Engineering*, vol. 27, no. 12, Article ID 04015049, 2015.

[2] S. P. Wu, P. C. Feng, H. L. Zhang, and J. Y. Yu, "Effect of organo-montmorillonite on aging properties of asphalt," *Construction and Building Materials*, vol. 23, no. 7, pp. 2636–2640, 2009.

[3] W. Zeng, S. Wu, J. Wen, and Z. Chen, "The temperature effects in aging index of asphalt during UV aging process," *Construction and Building Materials*, vol. 93, pp. 1125–1131, 2015.

[4] J. Hu, S. Wu, Q. Liu et al., "Effect of ultraviolet radiation in different wavebands on bitumen," *Construction and Building Materials*, vol. 159, pp. 479–485, 2018.

[5] W. Zeng, S. Wu, L. Pang et al., "Research on Ultra Violet (UV) aging depth of asphalts," *Construction and Building Materials*, vol. 160, pp. 620–627, 2018.

[6] J. Jin, Y. Gao, Y. Wu et al., "Rheological and adhesion properties of nano-organic palygorskite and linear SBS on the composite modified asphalt," *Powder Technology*, vol. 377, pp. 212–221, 2021.

[7] H. Yu, G. Deng, Z. Zhang, M. Zhu, M. Gong, and M. Oeser, "Workability of rubberized asphalt from a perspective of particle effect," *Transportation Research Part D: Transport and Environment*, vol. 91, Article ID 102712, 2021.

[8] M. Guo, M. Liang, A. Sreeram, A. Bhasin, and D. Luo, "Characterisation of rejuvenation of various modified asphalt binders based on simplified chromatographic techniques," *International Journal of Pavement Engineering*, pp. 1–11, 2021.

[9] J. Y. Yu, Y. S. Liang, and Z. G. Feng, "Investigation of ultraviolet ageing on rheological characteristics of bitumen," *Applied Mechanics and Materials*, vol. 71-78, pp. 1954–1957, 2011.

[10] Z. G. Feng, J. Y. Yu, H. L. Zhang, D. L. Kuang, and L. H. Xue, "Effect of ultraviolet aging on rheology, chemistry and morphology of ultraviolet absorber modified bitumen," *Materials and Structures*, vol. 46, no. 7, pp. 1123–1132, 2013.

[11] P. Cong, X. Wang, P. Xu, J. Liu, R. He, and S. Chen, "Investigation on properties of polymer modified asphalt containing various antiaging agents," *Polymer Degradation and Stability*, vol. 98, no. 12, pp. 2627–2634, 2013.

[12] S. Lv, X. Peng, C. Liu et al., "Aging resistance evaluation of asphalt modified by Buton-rock asphalt and bio-oil based on the rheological and microscopic characteristics," *Journal of Cleaner Production*, vol. 257, no. 6, p. 120589, 2020.

[13] W. Jiang, P. Li, W. Ye, J. Shan, Y. Li, and J. J. Xiao, "The effect and mechanism of La2O3 on the anti-ultraviolet aging characteristics of virgin bitumen," *Construction and Building Materials*, vol. 230, Article ID 116967, 2020.

[14] M. Guo, X. Liu, Y. Jiao, Y. Tan, and D. Luo, "Rheological characterization of reversibility between aging and rejuvenation of common modified asphalt binders," *Construction and Building Materials*, vol. 301, Article ID 124077, 2021.

[15] Q. Chen, C. Wang, S. Yu, Z. Song, H. Fu, and T. An, "Low-temperature mechanical properties of polyurethane-modified waterborne epoxy resin for pavement coating," *International Journal of Pavement Engineering*, pp. 1–13, 2022.

[16] H. Yu, X. Bai, G. Qian et al., "Impact of ultraviolet radiation on the aging properties of SBS-modified asphalt binders," *Polymers*, vol. 11, no. 7, p. 1111, 2019.

[17] L. D. Poulikakos, S. d. Santos, M. Bueno, S. Kuentzel, M. Hugener, and M. N. Partl, "Influence of short and long term aging on chemical, microstructural and macro-mechanical properties of recycled asphalt mixtures," *Construction and Building Materials*, vol. 51, pp. 414–423, 2014.

[18] M. Liang, X. Xin, W. Fan, H. Luo, X. Wang, and B. Xing, "Investigation of the rheological properties and storage stability of CR/SBS modified asphalt," *Construction and Building Materials*, vol. 74, pp. 235–240, 2015.